Acta Cryst. (1978). A**34**, 74–84

Investigation of Antiphase Domains in Lithium Ferrite by Analysis of the Broadened X-ray Diffraction Lines

BY R. W. CHEARY

NSW Institute of Technology, PO Box 123, *Broadway, New South Wales, Australia* 2007

AND N. W. GRIMES

*Physics Department, University of Aston, Birmingham B*4 7*ET, England*

(*Received* 28 *June* 1977; *accepted* 24 *July* 1977)

The formation and growth of antiphase domains in lithium ferrite has been investigated through an analysis of the X-ray diffraction line broadening. Calculations of the parameter $J'(0)/J(0)$ have been carried out by the method of Wilson & Zsoldos [*Proc. R. Soc. London*, (1966), A**290**, 508–514], for various boundary structure models with allowance being made for the presence of enantiomorphism. The experimental results indicate that the boundaries form predominantly on {110} planes, which is consistent with the principle of tetrahedral charge invariance. It has also been found that during the initial stages of growth the domain thickness distribution resembles a Gaussian curve, but as further growth occurs it takes on a truncated Cauchy-like character. The rate of this change is strongly correlated with the time of growth dependence of the mean domain thickness. Finally, an activation energy of $3{\cdot}1 \pm 0{\cdot}8$ eV was obtained for the growth process which is in reasonable agreement with the calculated value (2·53 eV).

Introduction

Lithium ferrite, $Fe[Li_{0{\cdot}5}Fe_{2{\cdot}5}]O_4$ is a ferrimagnetic oxide, belonging to the spinel family, which possesses a crystallographic order–disorder transition in the temperature range 735 to 765°C (Kato, 1958; Brunel & de Bergevin, 1964; Vishnevskii, Alapin, Lysak & Skripak, 1969) characterized by the space-group change cubic $P4_332$ (or $P4_132$) to cubic $Fd3m$ (Braun, 1952). In the disordered state the four Li^+ ions and twelve Fe^{3+} ions, of the eight molecules per unit cell, are statistically distributed over the octahedrally coordinated sites of the structure, but not entirely at random. The arrangement of the eight Fe^{3+} ions on the tetrahedrally coordinated sites and the O^{2-} ions is substantially unaffected by the transition.

The difference in calculated Coulomb energy between the ordered and randomly disordered forms of lithium ferrite is 111 kcal mole^{-1} (de Boer, van Santen & Verwey, 1950) which is many orders of magnitude larger than the thermal energy at the transition temperature. This being so, short-range order must persist in the disordered phase. Anderson (1956) suggested that this may be realized by an arrangement in which each tetrahedral group of nearest-neighbour octahedrally coordinated ions always comprises three Fe^{3+} ions and one Li^+ ion, a condition referred to as tetrahedral charge invariance. X-ray diffuse scattering measurements by Brunel & de Bergevin (1966) have since confirmed that this condition is rigidly adhered to in disordered lithium ferrite.

The development of order from the disordered structure occurs through the formation of contiguous antiphase domains. During this stage the X-ray diffraction pattern exhibits superlattice lines which are broadened and face-centred cubic lattice lines whose breadths are determined principally by the resolution function of the instrument and the X-ray emission profile (Cheary & Grimes, 1972*a*). However, unlike many other structures that form antiphase domains, such as Cu_3Au alloy, lithium ferrite possesses eight rather than four possible types of domain. This arises because the ordered structure within each domain may nucleate with equal probability according to the space group $P4_332$ or its enantiomorph $P4_132$ (Lefebvre, Portier & Fayard, 1974). Each of these alternative structures can then give rise to four domain types related to each other by one of the face centre translations $\frac{1}{2}\frac{1}{2}0$, $\frac{1}{2}0\frac{1}{2}$ and $0\frac{1}{2}\frac{1}{2}$.

Perfect long-range order is attained by domain growth, in which certain domains grow at the expense of adjacent domains until each crystallite consists of a single domain (Marcinkowski & Fisher, 1960; Yamaguchi, Watanabe & Ogawa, 1961). In Cu_3Au alloy, Poquette & Mikkola (1969) have shown that this process is diffusion controlled. Thus it would appear that the movement of domain boundaries is somewhat random and not unlike a random walk process with absorption. Consequently, each incremental increase in mean domain thickness D must be accompanied by the loss of a domain whose dimension immediately before absorption is of the order of a unit cell. This

implies that the fraction of domains having a thickness between 0 and dT will be approximately dT/D, that is, that the probability density function for the domain thickness distribution $f(T)$ at $T = 0$ will be $\sim 1/D$. This assessment is consistent with the results to be described here but not with those of Bessière, Bley, Calvayrac, Lefebvre & Fayard (1976) who estimated $f(0)$ for lithium ferrite as zero. It is worth mentioning, however, that this is probably not a real discrepancy as their analysis was based on a Fourier method which is particularly susceptible to systematic errors (Cheary & Grimes, 1972*b*). In other respects the results of Bessière *et al.* are broadly consistent with the present work, as are those of Lefebvre *et al.* (1974), which indicate that all possible types of adjacent domain are allowed and that the boundaries are not planar in the sense that each boundary is not defined by a single plane. However, this does not preclude the possibility that a particular boundary may be defined by a number of planes of a specific $\{hkl\}$ set each of which extends only over a restricted region of that boundary.

In the present investigation, the X-ray diffraction line-broadening analysis is extended beyond the work of Bessière *et al.* to examine further the form of the domain boundaries and domain thickness distribution in lithium ferrite. Finally, some consideration is given to the time and temperature kinetics of the growth process.

Experimental details

In our experiments, all the samples were prepared by the solid state reaction of reagent grade Li_2CO_3 with α-Fe_2O_3. Partially ordered specimens were formed from fully ordered specimens which were reheated up to 900 °C and allowed to come to equilibrium, after which time the temperature was reduced to a preset value just below the transition temperature for a specific period of time before being quenched in liquid nitrogen. In all, 16 partially ordered specimens were investigated together with one fully ordered sample which was used for reference purposes. The quenching conditions for the former were as follows:

Group 1. Four specimens quenched from temperatures of 745, 740, 735 and 725 °C after holding times of less than 10 min.

Group 2. Nine specimens quenched from 700 °C after holding times of 0, 0·5, 1, 5, 10, 20, 40, 60 and 140 min.

Group 3. Three specimens quenched from 730 °C after holding times of 1, 10 and 30 min.

X-ray diffraction patterns from all of these specimens exhibited the feature characteristic of a material containing antiphase domains namely, broadened superlattice lines together with sharp lattice lines. Only in the case of the fully ordered sample, were the superlattice lines of a sharpness comparable to that of the neighbouring lattice lines.

Subsequent evaluation of the breadths of the observed line profiles was carried out by variance analysis (Wilson, 1962, 1963) and values for the parameters $J'(0)/J(0)$ and $J''(0)/J(0)$ were estimated from the slopes and intercepts of the variance–range characteristics from the broadened profiles. To ensure reliable values for these parameters, allowance was made for a number of factors including the background contribution, the resolution function of the instrument and the emission profile, the presence of the $K\alpha$ satellite lines, the inverse-range-dependent term in the variance, angular factors and cross terms in the variance intercept (Cheary & Grimes, 1972*a*). Further details of the correction procedures are given in Langford (1968*a*, *b*) and Wilson (1965, 1970).

Table 1. *Experimental values of* $J'(0)/J(0) \times 10^4$ (Å^{-1}) *together with errors of measurement in parentheses*

Quenching temperature (°C)	Holding time (min)	110	210	211	310	320	321	421
725	<10	−118 (10)	−125 (7)	−117 (9)	−130 (9)	−129 (20)	–	−120 (18)
735	<10	−85 (5)	−88 (5)	−81 (6)	−88 (11)	−86 (13)	−90 (19)	−90 (11)
740	<10	−134 (6)	−132 (6)	−123 (7)	−135 (11)	−127 (15)	–	−135 (11)
745	<10	−97 (8)	−99 (6)	−102 (7)	−95 (19)	−92 (19)	−104 (23)	−88 (13)
700	0	−169 (18)	−202 (14)	−164 (17)	−165 (27)	–	–	−174 (26)
700	½	–	−166 (14)	–	–	–	–	–
700	1	−136 (14)	−160 (11)	−142 (12)	−148 (20)	–	–	−139 (24)
700	5	−147 (16)	−146 (13)	−132 (17)	−136 (24)	–	–	−144 (26)
700	10	–	−143 (12)	–	–	–	–	–
700	20	–	−137 (12)	–	–	–	–	–
700	40	–	−132 (9)	–	–	–	–	–
700	60	−127 (13)	−110 (10)	−116 (15)	−132 (20)	–	–	−114 (19)
700	140	−100 (9)	−105 (7)	−108 (10)	−95 (12)	–	–	−115 (18)
730	1	–	−173 (13)	–	–	–	–	–
730	10	–	−152 (12)	–	–	–	–	–
730	30	–	−97 (8)	–	–	–	–	–

Table 2. *Experimental values of* $J''(0)/J(0) \times 10^6$ ($Å^{-2}$) *together with errors of measurement in parentheses*

Quenching temperature (°C)	Holding time (min)	110	210	211	310	320	321	421
725	<10	145 (11)	154 (9)	136 (10)	178 (16)	152 (27)	–	141 (20)
735	<10	81 (4)	68 (4)	72 (6)	85 (10)	69 (11)	84 (18)	84 (11)
740	<10	131 (8)	137 (7)	117 (8)	145 (15)	135 (18)	–	147 (14)
745	<10	80 (7)	108 (6)	94 (7)	86 (17)	94 (17)	97 (25)	65 (12)
700	0	262 (27)	402 (28)	251 (25)	225 (35)	–	–	270 (47)
700	½	–	271 (21)	–	–	–	–	–
700	1	209 (18)	286 (18)	226 (16)	267 (27)	–	–	238 (32)
700	5	234 (22)	236 (18)	204 (22)	217 (30)	–	–	236 (35)
700	10	–	216 (16)	–	–	–	–	–
700	20	–	217 (16)	–	–	–	–	–
700	40	–	184 (13)	–	–	–	–	–
700	60	183 (16)	133 (11)	136 (17)	188 (25)	–	–	151 (20)
700	140	106 (9)	117 (8)	133 (12)	127 (11)			155 (22)

In this analysis $K'(0)/J(0)$ was assumed to be zero as the broadened profiles were symmetrical and not significantly displaced with respect to either the lattice lines or the sharp superlattice lines of the reference specimen. Moreover, the values for the variance slope and intercept from the lattice lines of the partially and fully ordered specimens were not significantly different which indicates that distortion at the antiphase domain boundaries is probably negligible.

As many of the broadened superlattice lines, particularly those at high angles were either very weak (*e.g.* 221 or 411/330) or overlapping onto neighbouring superlattice lines (*e.g.* 521 onto 520/432) or lattice lines (611/532 onto 620), variance analysis could only be carried out with reasonable accuracy on a restricted number of profiles, namely 110, 210, 211, 310, 320, 321 and 421. In certain samples even some of these could not be analysed satisfactorily. For some of the samples quenched from 700 and 730°C only the 210 profile, the most intense superlattice line, was measured.

The complete range of values for $J'(0)/J(0)$ and $J''(0)/J(0)$ derived from our observations are listed in Tables 1 and 2 together with the thermal treatment to which the corresponding samples were subjected. The quoted experimental errors reflect the range of values for different background levels over which the variance–range graphs in the 'linear region' were visually indistinguishable from a straight line. In all of the profiles analysed these errors were much larger than those arising from counting statistics (Wilson, 1967). Indeed, for some samples the breadth of the superlattice lines was so extensive that correction for the resolution function and emission profile was hardly necessary.

Analysis of antiphase domain boundary structure

With the possible exception of the specimens quenched from 700°C after periods of 0 and ½ minute, the experimental values of $J'(0)/J(0)$ do not vary appreciably with *hkl* within the errors quoted. For interpretation, therefore, the approach adopted has been to develop various models for the domain boundary structure using the tetrahedral charge invariance principle (Anderson, 1956) as the condition which must be upheld at the boundary. As this principle is adhered to even in the disordered state, any boundaries which give

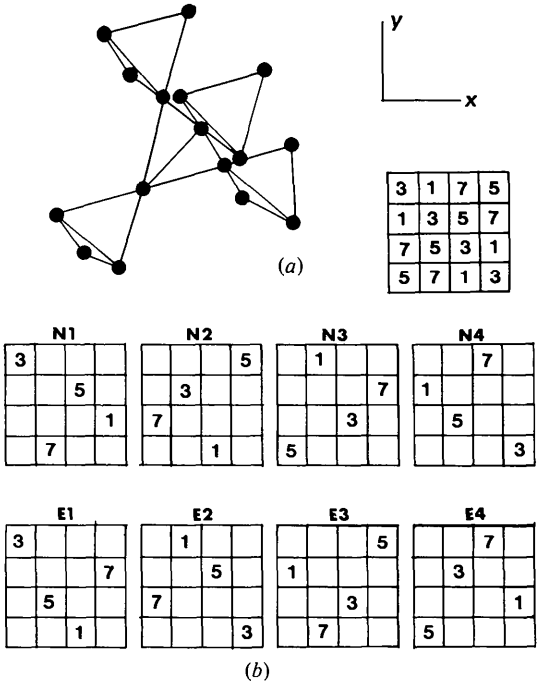

Fig. 1. (*a*) Arrangement of octahedral ions in each unit cell. In this (001) projection of the structure the numbers represent the *z* coordinates of these ions expressed in eighths of the unit-cell parameters. (*b*) Positions of Li^+ ions for each type of domain, four normal structures (*N*) and four enantiomorphic structures (*E*).

rise to more than, or less than, one Li^+ in each tetrahedral group of octahedral ions, will be very unstable.

Fortunately, it is a relatively simple matter to modify the method of Wilson & Zsoldos (1966) to allow for the presence of enantiomorphic domains in the calculation of $J'(0)/J(0)$. In what follows, we shall refer to the structure corresponding to the space group $P4_332$ as the normal structure and that corresponding to $P4_132$ as the enantiomorphic structure and label the domains associated with each of these as $N1$ to $N4$, and $E1$ to $E4$, respectively. The positions of the Li^+ ions in each of these domain types (Lefebvre *et al.*, 1974) are listed in Table 3 and illustrated in Fig. 1 together with the octahedral cation structure in each unit cell.

Table 3. *Positions of* Li^+ *ions in the different domain types*

$N1$	$\frac{1}{8}\frac{7}{8}\frac{3}{8}$	$\frac{3}{8}\frac{1}{8}\frac{7}{8}$	$\frac{5}{8}\frac{5}{8}\frac{5}{8}$	$\frac{7}{8}\frac{3}{8}\frac{1}{8}$	
$N2$	$\frac{1}{8}\frac{3}{8}\frac{7}{8}$	$\frac{3}{8}\frac{5}{8}\frac{3}{8}$	$\frac{5}{8}\frac{1}{8}\frac{1}{8}$	$\frac{7}{8}\frac{7}{8}\frac{5}{8}$	$= N1 + 0\frac{1}{2}\frac{1}{2}$
$N3$	$\frac{1}{8}\frac{1}{8}\frac{5}{8}$	$\frac{3}{8}\frac{7}{8}\frac{1}{8}$	$\frac{5}{8}\frac{3}{8}\frac{3}{8}$	$\frac{7}{8}\frac{5}{8}\frac{7}{8}$	$= N1 + \frac{1}{2}\frac{1}{2}0$
$N4$	$\frac{1}{8}\frac{5}{8}\frac{1}{8}$	$\frac{3}{8}\frac{3}{8}\frac{5}{8}$	$\frac{5}{8}\frac{7}{8}\frac{7}{8}$	$\frac{7}{8}\frac{1}{8}\frac{3}{8}$	$= N1 + \frac{1}{2}0\frac{1}{2}$
$E1$	$\frac{1}{8}\frac{7}{8}\frac{3}{8}$	$\frac{3}{8}\frac{3}{8}\frac{5}{8}$	$\frac{5}{8}\frac{1}{8}\frac{1}{8}$	$\frac{7}{8}\frac{5}{8}\frac{7}{8}$	
$E2$	$\frac{1}{8}\frac{3}{8}\frac{7}{8}$	$\frac{3}{8}\frac{7}{8}\frac{1}{8}$	$\frac{5}{8}\frac{5}{8}\frac{5}{8}$	$\frac{7}{8}\frac{1}{8}\frac{3}{8}$	$= E1 + 0\frac{1}{2}\frac{1}{2}$
$E3$	$\frac{1}{8}\frac{5}{8}\frac{1}{8}$	$\frac{3}{8}\frac{1}{8}\frac{7}{8}$	$\frac{5}{8}\frac{3}{8}\frac{3}{8}$	$\frac{7}{8}\frac{7}{8}\frac{5}{8}$	$= E1 + \frac{1}{2}\frac{1}{2}0$
$E4$	$\frac{1}{8}\frac{1}{8}\frac{5}{8}$	$\frac{3}{8}\frac{5}{8}\frac{3}{8}$	$\frac{5}{8}\frac{7}{8}\frac{7}{8}$	$\frac{7}{8}\frac{3}{8}\frac{1}{8}$	$= E1 + \frac{1}{2}0\frac{1}{2}$

For all types of domain the modulus of the structure factor $|F|$ for each of the superlattice lines has the form

$$|F| = C[f(Fe^{3+}) - f(Li^+)],$$

where the constant C is a function of hkl, so that if we write $F_{N1} = F$ then $F_{E1} = F\exp(j\varphi_{hkl})$ where φ_{hkl} is the phase difference between the $N1$ and $E1$ structures, and we have

$$F_{N2} = (-1)^{k+l}F; \quad F_{E2} = (-1)^{k+l}F\exp(j\varphi_{hkl})$$
$$F_{N3} = (-1)^{h+k}F; \quad F_{E3} = (-1)^{h+k}F\exp(j\varphi_{hkl})$$
$$F_{N4} = (-1)^{h+l}F; \quad F_{E4} = (-1)^{h+l}F\exp(j\varphi_{hkl}).$$

Let $p_T(X/Y)$ be the probability of finding a cell of type X at a distance T in the $[hkl]$ direction, given a cell of type Y at the origin $T = 0$. Then, following Wilson & Zsoldos and assuming that normal and enantiomorphic unit cells are equally abundant, $J(T)$ the mean value of FF^* for cells separated by a distance T in the $[hkl]$ direction, will be given by

$$\begin{aligned} J(T) = {} & |F|^2\{p_T(N1/N1) + (-1)^{k+l}p_T(N2/N1) \\ & + (-1)^{h+k}p_T(N3/N1) + (-1)^{h+l}p_T(N4/N1)\} \\ & + |F|^2\cos\varphi_{hkl}\{p_T(E1/N1) \\ & + (-1)^{k+l}p_T(E2/N1) \\ & + (-1)^{h+k}p_T(E3/N1) + (-1)^{h+l}p_T(E4/N1)\}. \quad (1) \end{aligned}$$

Let α_2 to α_4 and β_1 to β_4 be the chances per unit distance of T in the $[hkl]$ direction of structures $N2$ to $N4$ and $E1$ to $E4$ respectively changing to $N1$; then by analogy once more with Wilson & Zsoldos, $J'(0)/J(0)$ will be given by

$$\begin{aligned} \frac{J'(0)}{J(0)} = {} & -\{\alpha_2[1 - (-1)^{k+l}] + \alpha_3[1 - (-1)^{h+k}] \\ & + \alpha_4[1 - (-1)^{h+l}] + \beta_1(1 - \cos\varphi_{hkl}) \\ & + \beta_2[1 - (-1)^{k+l}\cos\varphi_{hkl}] \\ & + \beta_3[1 - (-1)^{h+k}\cos\varphi_{hkl}] \\ & + \beta_4[1 - (-1)^{h+l}\cos\varphi_{hkl}]\}, \quad (2) \end{aligned}$$

where for lithium ferrite, $\varphi_{hkl} = \pm n\pi/2$ with n an integer related to h, k and l. Note that, although the calculation of $J(T)$ according to the method of Wilson & Zsoldos assumes a particular form for the domain thickness distribution $f(T)$, this does not affect equation (2) as $J'(0)/J(0)$ is independent of $f(T)$ (Wilson, 1958).

Thus, the problem may be reduced to one of determining the variation of the α_i and β_i with hkl and with $\{HKL\}$, the indices of the planes forming the domain boundaries. However, to be realistic the model must be similar to that with non-planar and statistically isotropic boundaries in which $J'(0)/J(0)$ is independent of hkl and has the form

$$\frac{J'(0)}{J(0)} = -\frac{8}{7D} \quad \text{with all } \alpha_i = \beta_i = \frac{1}{7D} \quad (3)$$

and D = mean domain thickness. It is worth mentioning that this form of relation for $J'(0)/J(0)$ is also applicable to planar models when all types of adjacent domain are allowed, although D is then a function of hkl.

To determine the restrictions imposed on the types of adjacent domain by the tetrahedral invariance condition, boundaries comprising $\{100\}$, $\{110\}$, $\{111\}$ and $\{210\}$ planes were studied. This was done by examining the compatibility of the various structures across each of the above boundary planes at all possible locations within the unit cell. In doing this, it was only necessary to determine the allowed changes in the x direction, as those in the y and z directions can be derived from the symmetry of the structure.

At first only changes for which the boundaries are strictly contiguous were considered and as a result it was found that not all types of adjacent domain are allowed. For each of the $\{100\}$ type boundaries only six of the seven possible changes can occur from each particular structure, namely two of the same type and four of the opposite type [*e.g.* $E1 \rightarrow N1$, $N2$, $N3$, $N4$, $E3$ and $E4$ across (100) planes]. Across $\{110\}$ planes the situation is more restrictive in that only three possible changes are allowed across each particular boundary [*e.g.* $N2 \rightarrow N1$, $E1$ and $E2$ across (011) planes]. However, if all the changes which are allowed across $\{110\}$ planes in the x direction are considered together [*i.e.* across (110), $(1\bar{1}0)$, (101) and $(10\bar{1})$ planes] the situation is identical to that of the (100) boundaries. This is also the case in the y and z direc-

tions in relation to the allowed changes across the (010) and (001) planes respectively. The allowed changes from the $N1$ structure across the (100) and (1$\bar{1}$0) planes giving contiguous adjacent domains are illustrated in Fig. 2 in terms of the projected octahedral cation structure. Across each (111) boundary only one type of change is allowed and this is always of the kind normal → enantiomorphic or *vice-versa*. For example, across the (111) planes the complete list of possible changes is $N1 \rightleftharpoons E2$, $N2 \rightleftharpoons E1$, $N3 \rightleftharpoons E4$ and $N4 \rightleftharpoons E3$. In the case of {210} boundaries all types of adjacent domains violate the tetrahedral invariance condition.

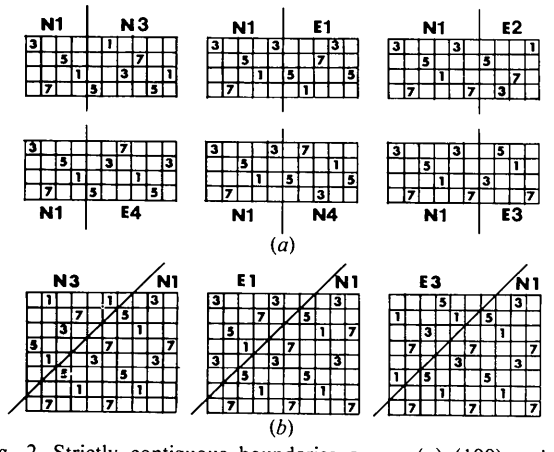

Fig. 2. Strictly contiguous boundaries across (*a*) (100) and (*b*) (1$\bar{1}$0) planes; types allowed by tetrahedral invariance condition.

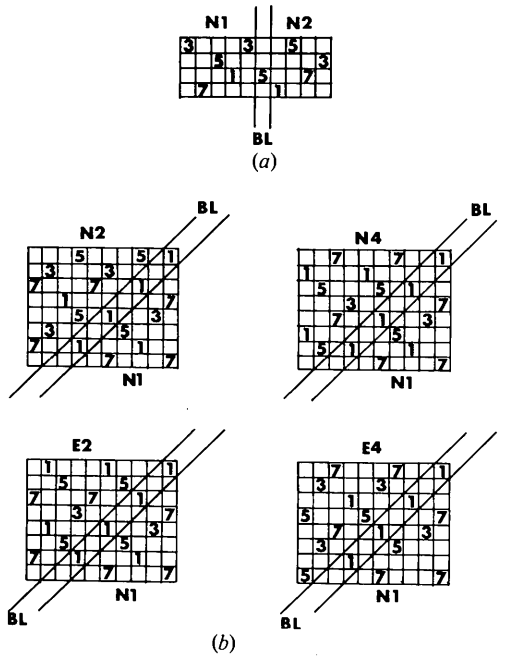

Fig. 3. Additional (*a*) (100) and (*b*) (110) boundary types allowed by tetrahedral invariance condition when an intermediate layer is introduced at the boundary. BL = Boundary layer.

When the restriction of strictly contiguous adjacent domains is relaxed further types of change are allowed. One way of forming nearly contiguous domains satisfying the tetrahedral invariance principle is to introduce a boundary layer in which the Li^+ ions are out of position with respect to the structures on each side of the layer. In this manner it is possible to form all the previously disallowed boundary changes across {100} and {110} planes, and thus the state observed by Lefebvre *et al.* (1974), of all adjacent domain types being allowed, could by achieved. Boundaries involving boundary layers are illustrated in Fig. 3 using as examples those changes forbidden under the contiguous boundary conditions of Fig. 2. Introducing a single intervening layer on {111} or {210} boundaries, however, does not increase the number of allowed adjacent domain types in these cases.

The forms of the α and β coefficients for each of the various allowed boundary models are summarized in Tables 4 and 5. In Table 4, δ_{HKL} (or δ'_{HKL}) is the probability of change per unit length in the $[HKL]$ direction for boundaries on (HKL) planes, so that for a specific change the probability is δ_{HKL}/n where n is the number of allowed changes. For the sake of completeness, the {111} boundary model, with all adjacent domains allowed, is also included. The expressions for $J'(0)/J(0)$ in terms of the α and β coefficients are given in Table 5 together with the phase differences φ_{hkl} between the normal and enantiomorphic structures $N1$ and $E1$ calculated from the corresponding structure factors.

Because the tetrahedral invariance condition may be satisfied across both {100} and {110} and, to a lesser extent, across {111} boundaries, the possibility of a hybrid boundary structure also exists. Further forms for $J'(0)/J(0)$ with only one unknown parameter were therefore constructed on the basis that:

(*a*) $\left(\frac{J'(0)}{J(0)}\right)_{HKL,H'K'L'}$ for boundaries comprising either $\{HKL\}$ or $\{H'K'L'\}$ is given by

$$\left(\frac{J'(0)}{J(0)}\right)_{HKL,H'K'L'} = \left(\frac{J'(0)}{J(0)}\right)_{HKL} + \left(\frac{J'(0)}{J(0)}\right)_{H'K'L'}$$

(Wilson & Zsoldos, 1966).

(*b*) For any specific change allowed by the tetrahedral invariance condition, the boundaries associated with the change are randomly distributed between the component planes. Thus, the relation between the probabilities δ_{HKL} and $\delta_{H'K'L'}$ can be obtained from the equation:

(number of possible $\{HKL\}$ boundaries in $[hkl]$ direction)/(number of possible $\{H'K'L'\}$ boundaries in $[hkl]$ direction)

= (actual number of $\{HKL\}$ boundaries in the $[hkl]$ direction)/(actual number of $\{H'K'L'\}$ boundaries in the $[hkl]$ direction),

Table 4. *Form of α and β coefficients for various boundary models*

h,k,l are positive and arranged in the order $h \geq k \geq l$ and $N = h^2 + k^2 + l^2$.

Model	Boundary (*HKL*)	Cosine factor	Probability of change from *N*1 to *N*2	*N*3	*N*4	*E*1	*E*2	*E*3	*E*4	α and β coefficients
{100} contiguous only	100	$h/\sqrt{N}$	0	$\frac{\delta_{100}}{6}$	$\frac{\delta_{100}}{6}$	$\frac{\delta_{100}}{6}$	$\frac{\delta_{100}}{6}$	$\frac{\delta_{100}}{6}$	$\frac{\delta_{100}}{6}$	$\alpha_2 = (k+l)\,\delta_{100}/6\sqrt{N}$
	010	$k/\sqrt{N}$	$\frac{\delta_{100}}{6}$	$\frac{\delta_{100}}{6}$	0	$\frac{\delta_{100}}{6}$	$\frac{\delta_{100}}{6}$	$\frac{\delta_{100}}{6}$	$\frac{\delta_{100}}{6}$	$\alpha_3 = (h+k)\,\delta_{100}/6\sqrt{N}$
	001	$l/\sqrt{N}$	$\frac{\delta_{100}}{6}$	0	$\frac{\delta_{100}}{6}$	$\frac{\delta_{100}}{6}$	$\frac{\delta_{100}}{6}$	$\frac{\delta_{100}}{6}$	$\frac{\delta_{100}}{6}$	$\alpha_4 = (h+l)\,\delta_{100}/6\sqrt{N}$
										$\beta_1=\beta_2=\beta_3=\beta_4=\frac{(h+k+l)}{6\sqrt{N}}\,\delta_{100}$
{110} contiguous only	011	$(k+l)/\sqrt{2N}$	$\frac{\delta_{110}}{3}$	0	0	$\frac{\delta_{110}}{3}$	$\frac{\delta_{110}}{3}$	0	0	$\alpha_2 = 2\delta_{110}\,k/3\sqrt{2N}$
	110	$(h+k)/\sqrt{2N}$	0	$\frac{\delta_{110}}{3}$	0	0	$\frac{\delta_{110}}{3}$	0	$\frac{\delta_{110}}{3}$	$\alpha_3=\alpha_4=\beta_1=\beta_3=\frac{2\delta_{110}\,h}{3\sqrt{2N}}$
	101	$(h+l)/\sqrt{2N}$	0	0	$\frac{\delta_{110}}{3}$	0	$\frac{\delta_{110}}{3}$	$\frac{\delta_{110}}{3}$	0	
	$01\bar{1}$	$(k-l)/\sqrt{2N}$	$\frac{\delta_{110}}{3}$	0	0	0	0	$\frac{\delta_{110}}{3}$	$\frac{\delta_{110}}{3}$	$\beta_2=\frac{2\delta_{110}(h+k+l)}{3\sqrt{2N}}$
	$1\bar{1}0$	$(h-k)/\sqrt{2N}$	0	$\frac{\delta_{110}}{3}$	0	$\frac{\delta_{110}}{3}$	0	$\frac{\delta_{110}}{3}$	0	
	$10\bar{1}$	$(h-l)/\sqrt{2N}$	0	0	$\frac{\delta_{110}}{3}$	$\frac{\delta_{110}}{3}$	0	0	$\frac{\delta_{110}}{3}$	$\beta_4=\frac{2\delta_{110}(h+k-l)}{3\sqrt{2N}}$
{111} contiguous only	111	$(h+k+l)/\sqrt{3N}$	0	0	0	0	δ_{111}	0	0	$\alpha_2=\alpha_3=\alpha_4=0$
	$1\bar{1}\bar{1}$	$\lvert h-k-l\rvert/\sqrt{3N}$	0	0	0	δ_{111}	0	0	0	$\beta_1=\delta_{111}(h+k+l)/\sqrt{3N}$
	$1\bar{1}1$	$(h-k+l)/\sqrt{3N}$	0	0	0	0	0	δ_{111}	0	$\beta_2=\delta_{111}\lvert h-k-l\rvert/\sqrt{3N}$
	$11\bar{1}$	$(h+k-l)/\sqrt{3N}$	0	0	0	0	0	0	δ_{111}	$\beta_3=\delta_{111}(h-k+l)/\sqrt{3N}$
										$\beta_4=\delta_{111}(h+k-l)/\sqrt{3N}$
{100} all boundary types allowed	100 010 001	$h/\sqrt{N}$ $k/\sqrt{N}$ $l/\sqrt{N}$	$\delta'_{100}/7$ in all cases							$\alpha_2=\alpha_3=\alpha_4=\beta_1$ $=\beta_2=\beta_3=\beta_4$ $=\frac{(h+k+l)\,\delta'_{100}}{7\sqrt{N}}$
{110} all boundary types allowed	011 110 101 $01\bar{1}$ $1\bar{1}0$ $10\bar{1}$	$(k+l)/\sqrt{2N}$ $(h+k)/\sqrt{2N}$ $(h+l)/\sqrt{2N}$ $(k-l)/\sqrt{2N}$ $(h+k)/\sqrt{2N}$ $(h-l)/\sqrt{2N}$	$\delta'_{110}/7$ in all cases							$\alpha_2=\alpha_3=\alpha_4=\beta_1$ $=\beta_2=\beta_3=\beta_4$ $=\frac{(4h+2k)\,\delta'_{110}}{7\sqrt{2N}}$
{111} all boundary types allowed	111 $\bar{1}\bar{1}1$ $1\bar{1}1$ $11\bar{1}$	$(h+k+l)/\sqrt{3N}$ $\lvert h-k-l\rvert/\sqrt{3N}$ $(h-k+l)/\sqrt{3N}$ $(h+k-l)/\sqrt{3N}$	$\delta'_{111}/7$ in all cases							$\alpha_2=\alpha_3=\alpha_4=\beta_1$ $=\beta_2=\beta_3=\beta_4$ $=\frac{4\delta'_{111}\,h}{7\sqrt{3N}}$ $(h \geq k+l)$

from which the results

$$\delta_{100}=\frac{\delta_{110}}{\sqrt{2}}=\frac{\delta_{111}}{\sqrt{3}} \text{ are obtained.}$$

Models corresponding to these conditions were parameterized in terms of δ_{100} and included,

(i) {100} + {110}, strictly contiguous boundaries.

(ii) {100} + {110}, all adjacent domains allowed.

(iii) {100}, all adjacent domains allowed + {111}, strictly contiguous boundaries.

(iv) {110}, all adjacent domains allowed + {111}, strictly contiguous boundaries.

(v) {100} + {110}, all adjacent domains allowed + {111}, strictly contiguous boundaries.

To determine the extent to which the different models could be fitted to the experimental results a least

squares procedure was adopted in which the root mean square fit Δ_{HKL}, for a particular specimen and $\{HKL\}$ model, expressed as a percentage, was obtained from

$$\Delta_{HKL} = 100\left[\sum_{hkl} w_{hkl}\left(\frac{\delta^{hkl}_{HKL}}{\langle\delta_{HKL}\rangle} - 1\right)^2 \Big/ \sum_{hkl} w_{hkl}\right]^{1/2}$$

where δ^{hkl}_{HKL} is the value of δ_{HKL} given by the hkl line for the $\{HKL\}$ model, $\langle\delta_{HKL}\rangle$ is the weighted mean value of δ_{HKL} for a particular specimen and w_{hkl} is the weighting chosen to be the reciprocal of the error, expressed as a percentage, given in Table 1. The results of these calculations are presented in Table 6. Also included, for comparison, is the fit to the isotropic non-planar boundary model.

As Table 6 shows, the most consistent best fit with planar boundaries (six out of nine samples) is provided by the {110} model with all types of adjacent domain allowed. For the other three samples the best fit is obtained with one of the hybrid models, but even in these cases {110} planes comprise one of the component boundaries. Also, only one sample gave a best fit to the isotropic non-planar boundary model. It is worth remarking that the poor fit of the models with either strictly contiguous boundaries or {100} and/or {111} boundaries with all types of adjacent domain allowed was expected as these models predict marked changes in $J'(0)/J(0)$ with hkl. To minimize the effects of experimental errors, the average values of $J'(0)/J(0)$ over all nine samples for the 110, 210, 211, 310 and 421 diffraction lines were calculated and these proved once again to be in excellent agreement with the {110} model as shown in the last column of Table 6. Indeed, on this basis, the r.m.s. fit would appear to be substantially better for this model than for the other planar models and also, though to a lesser extent, than for the isotropic non-planar model.

Owing to the limited accuracy of the present data, the fitting of two parameter hybrid models, such as {100} + {110} boundaries or {110} + isotropic non-planar boundaries, was not considered. However, models such as these with the {110} boundaries playing a predominant role are a distinct possibility. It is well known, for instance, that lithium ferrite tends to lose a small proportion of its Li^+ ions at elevated temperature with the subsequent conversion of some of the Fe^{3+} ions to Fe^{2+} ions (Pointon & Saull, 1969). In such circumstances the tetrahedral invariance condition may not apply over localized regions of the crystal and different boundary structures may form. The electron micrograph analysis of Lefebvre *et al.* could well be explained by this effect. In addition, there is the possibility that more than one member of the {110} set of planes, together with a lesser proportion of {100} and {111} planes, may contribute to each individual boundary.

Table 5. *Form of $J'(0)/J(0)$ for measured superlattice reflections from lithium ferrite in terms of the α and β coefficients where φ_{hkl} is the phase difference between the normal and enantiomorphic structures, N1 and E1*

$h\,k\,l$	φ_{hkl}	$-J'(0)/J(0)$
1 1 0	π	$2(\alpha_2 + \alpha_4 + \beta_1 + \beta_3)$
2 1 0	$\pi/2$	$2(\alpha_2 + \alpha_3) + \beta_1 + \beta_2 + \beta_3 + \beta_4$
2 1 1	0	$2(\alpha_3 + \alpha_4 + \beta_3 + \beta_4)$
3 1 0	0	$2(\alpha_2 + \alpha_4 + \beta_2 + \beta_4)$
3 2 0	$\pi/2$	$2(\alpha_3 + \alpha_4) + \beta_1 + \beta_2 + \beta_3 + \beta_4$
3 2 1	0	$2(\alpha_2 + \alpha_3 + \beta_2 + \beta_3)$
4 2 1	$\pi/2$	$2(\alpha_2 + \alpha_4) + \beta_1 + \beta_2 + \beta_3 + \beta_4$

Table 6. *Root-mean-square fit of various domain boundary models to experimental values for $J'(0)/J(0)$*

Results are expressed as percentages. $\{HKL\}C$ refers to $\{HKL\}$ boundaries which are strictly contiguous and without boundary layers and $\{HKL\}A$ refers to boundaries at which all types of adjacent domain are allowed. The asterisk denotes planar model of best fit.

	Sample									
Model	725† <10‡	735 <10	740 <10	745 <10	700 0	700 1	700 5	700 60	700 140	Fit to average $J'(0)/J(0)$
{100}C	16·2	14·2	15·3	11·7	16·0	15·6	14·5	17·5	9·1	14·2
{110}C	7·6	9·9	12·2	12·0	10·2	7·1	12·6	15·3	11·3	9·7
{111}C	7·4	47·3	10·9	50·0	10·2	7·1	13·6	15·3	11·3	9·7
{100}C + {110}C	7·6	9·3	11·0	9·2	10·5	8·9	12·6	13·7	6·7	7·9
{100}A	12·3	10·3	10·6	8·4	14·9	13·5	10·8	12·4	6·1	10·6
{110}A	2·2*	2·1*	3·0*	7·1	6·6*	4·6	3·7*	8·1*	7·3	1·6*
{111}A	7·4	9·0	10·9	11·0	9·9	7·1	12·6	15·3	11·3	9·7
{100}A + {110}A	5·6	4·2	4·8	4·7*	9·2	7·0	5·2	8·4	3·6*	3·7
{100}A + {111}C	7·0	9·6	7·6	10·5	8·8	8·1	8·6	10·7	4·2	6·4
{110}A + {111}C	2·3	8·4	5·0	11·4	10·9	3·9*	6·3	9·5	7·8	3·7
{100}A + {110}A + {111}C	4·2	5·5	4·9	7·3	6·9	5·7	5·9	8·9	4·5	3·4
Isotropic non-planar	4·1	3·5	3·5	4·7	8·8	6·3	4·3	6·9	5·7	2·4

† Quenching temperature (°C). ‡ Holding time (min).

Consideration of the manner by which domain boundaries migrate lends further support to a hybrid model of allowed planar boundaries with a high proportion of {110} boundaries. As illustrated in Fig. 4, (100) and (1$\bar{1}$0) boundaries between the $N1$ and $N3$ structures are only allowed by the tetrahedral invariance condition across specific planes within the unit cell. In order for the (1$\bar{1}$0) boundary to move to its next allowed position, four Li^+ ion and Fe^{3+} ion interchanges have to occur as opposed to only two interchanges for the (100) boundary. {110} boundaries therefore will tend to be less mobile than {100} boundaries so that a structure originally consisting of a random mixture of these boundaries will eventually develop an excess of {100} boundaries as domain growth occurs.

Analysis of domain thickness distribution and kinetics of growth

As the antiphase domains in lithium ferrite are described satisfactorily by a model in which each possible type of adjacent domain is equally probable, $J''(0)/J(0)$ may be expressed in terms of the domain thickness distribution $f(T)$ as (Wilson, 1963)

$$\frac{J''(0)}{J(0)} = \left(\frac{J'(0)}{J(0)}\right)^2 f(0)\, D_{hkl},$$

where D_{hkl} is the mean domain thickness in the $[hkl]$ direction. When the probability of a change per unit length from one domain to the next is independent of the size of the domain (the random model), $f(T)$ is given by the exponential distribution (Wilson, 1943)

$$f_R(T) = \frac{1}{D_{hkl}} \exp\left(-\frac{T}{D_{hkl}}\right).$$

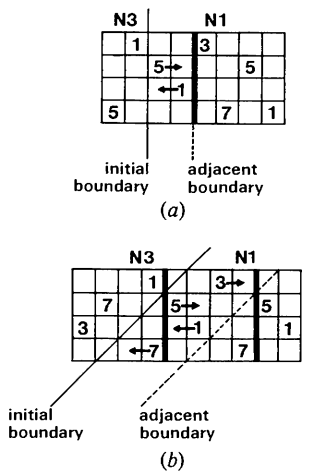

Fig. 4. Shifts of Li^+ ions in the movement of a boundary between adjacent allowed (100) and (1$\bar{1}$0) planes. (*a*) 100 migration, (*b*) 1$\bar{1}$0 migration.

Thus, $J''(0)/J(0)$ may also be expressed as

$$\frac{J''(0)}{J(0)} = \left(\frac{J'(0)}{J(0)}\right) \frac{f(0)}{f_R(0)}.$$

For values of $f(0)/f_R(0) < 1$ the proportion of very small and very large domains will be less than a random distribution of similar mean domain thickness. Consequently, the domains will be more uniform in size with a smaller variance than the random distribution. On the other hand, when $f(0)/f_R(0) > 1$ the proportion of very small and very large domains will be increased and the variance will tend to be greater than the random distribution.

Two such distributions possessing these properties are:

(i) the Gaussian distribution

$$f(T) = \frac{2}{\pi D_{hkl}} \exp\left(-\frac{T^2}{\pi D_{hkl}^2}\right); \quad \frac{f(0)}{f_R(0)} = 0{\cdot}637;$$

(ii) the truncated Cauchy distribution

$$f(T) = \frac{A}{D_{hkl}[1 + (T/\varepsilon)^2]} \qquad T \le T_{max}$$

$$f(T) = 0 \qquad T > T_{max}$$

which for $T_{max} = 20\varepsilon$ ($\simeq 40 D_{hkl}$) gives $A = f(0)/f_R(0) = 1{\cdot}30$. For this distribution values of $f(0)/f_R(0) < 1$ can be obtained by choosing a smaller T_{max}.

The actual form of these distributions is shown in Fig. 5 in relation to the random model distribution.

In our experiments, results were obtained consistent with approximations to each of the above distributions. This is illustrated in Fig. 6 where $|J'(0)/J(0)|$ is plotted against $[J''(0)/J(0)]^{1/2}$ for each of the samples together with the expected variation for each type of distribution. Nearly all of the samples examined

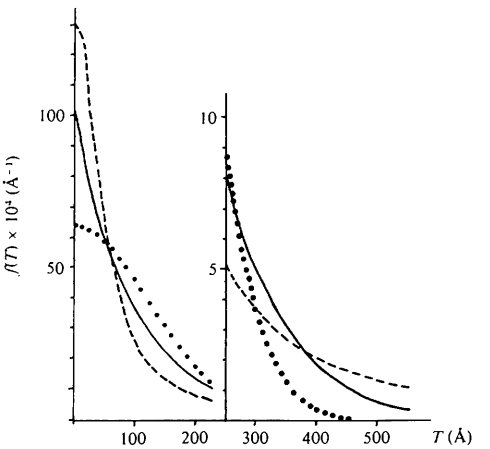

Fig. 5. Comparison of types of domain thickness distribution, each with the same mean domain thickness of 100 Å. —— Exponential distribution, ··· Gaussian distribution, – – – truncated Cauchy distribution.

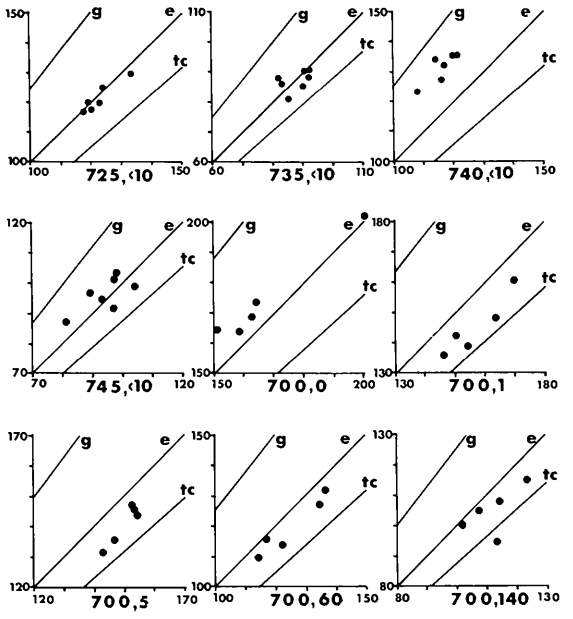

Fig. 6. Plots of experimental values for $|J'(0)/J(0)| \times 10^4$ Å^{-1} (vertical axis) against $[J''(0)/J(0)]^{1/2} \times 10^4$ Å^{-1} (horizontal axis). Each specimen is denoted by its quenching temperature in °C and holding time in minutes. The solid lines indicate relationships for various types of domain thickness distribution (*i.e.* *g* Gaussian, *e* exponential and tc truncated Cauchy distributions respectively).

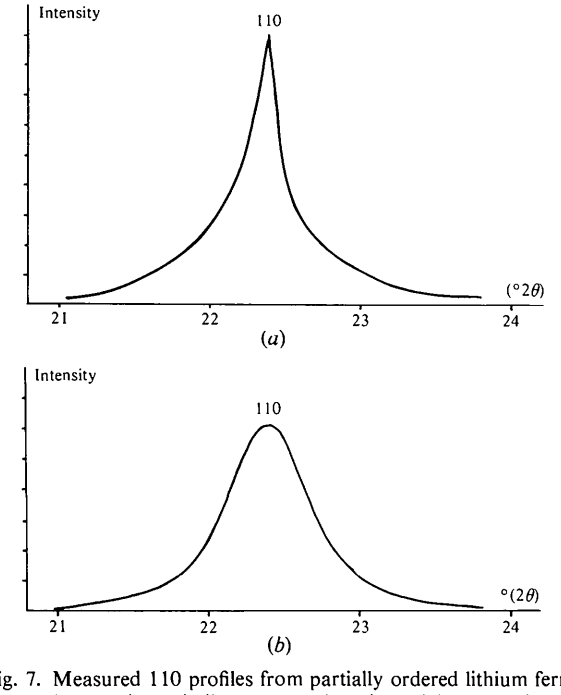

Fig. 7. Measured 110 profiles from partially ordered lithium ferrite samples having similar mean domain thicknesses (<10% difference) and similar integrated intensities, but different domain thickness distributions. (*a*) Sample 700°C, 5 min – Cauchy-like distribution. (*b*) Sample 740°C, <10 min – Gaussian-like distribution.

indicated a domain thickness distribution which in terms of $f(0)$, was within ±20% of the random model. However, in the majority of cases, the plotted points tend to lie either completely above the random line or completely below it and this is believed to be a real effect. For example, the shape of the X-ray diffraction profiles from those samples indicating a truncated Cauchy-like distribution was distinctly different from those exhibiting Gaussian-like characteristics. An example of this difference is given in Fig. 7.

For those samples quenched from 700°C there is a definite trend in the values deduced for $f(0)/f_R(0)$ as a function of time (see Fig. 8). It should be emphasized, however, that the major systematic errors associated with variance analysis (*i.e.* wrongly estimated satellite correction, non-linear terms in the variance–range function and wrongly estimated background correction) do not influence the estimation of $f(0)/f_R(0)$ to any great extent. In each case, the effect of an error is to increase (or decrease) $|J'(0)/J(0)|$ and $J''(0)/J(0)$ in unison and as a result the value derived for $f(0)/f_R(0)$ remains more or less constant. Moreover, effects arising from small particle size, strain and stacking faults appeared to be negligible as the lattice lines from the partially ordered specimens were equally as sharp as those from the ordered specimen. It is concluded therefore, that the time dependence of $f(0)/f_R(0)$ indicates that the initial state ($t = 0$) in lithium ferrite is best

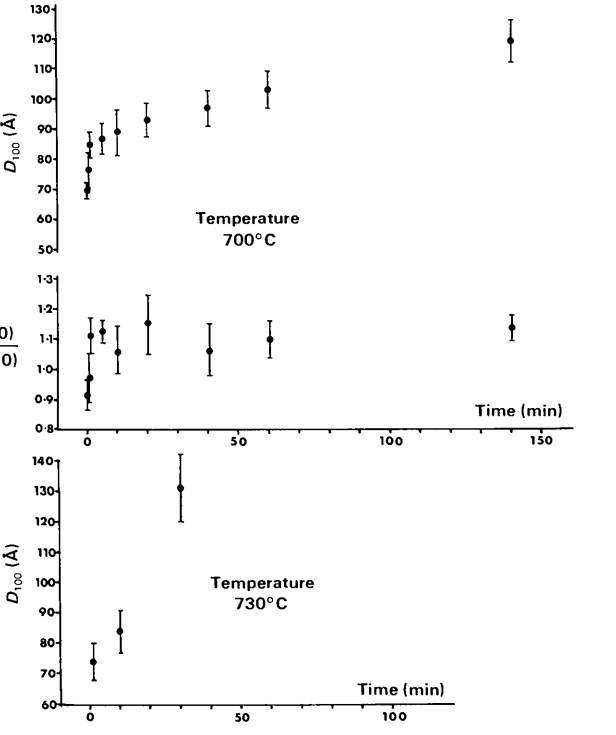

Fig. 8. Experimental values for D_{100}, the mean domain thickness in the [100] direction (given by $\delta_{110}\sqrt{2}/4$) and $f(0)/f_R(0)$ as a function of time.

described by a Gaussian-like distribution [$f(0)/f_R(0) \sim 0{\cdot}9$], but that, as domain growth occurs, this situation rapidly changes and after approximately one minute the distribution stabilizes at $f(0)/f_R(0) \sim 1{\cdot}1$ corresponding to a Cauchy-like distribution. Clearly, during the initial stages of growth there are very few large domains – hence the tendency towards a Gaussian distribution – but as growth proceeds large domains develop and, as a consequence, the domain thickness distribution changes.

This pattern of behaviour is strongly correlated with that of the mean domain thickness D_{hkl} which also exhibits a very rapid initial change ($t \leq 1$ minute). The time dependence of D_{100}, obtained from the average values of δ_{110} for each specimen is illustrated in Fig. 8 for both 700 and 730°C and analysis of the former shows that no simple relation can be found for the complete range of times investigated. However, for $t \geq 1$ minute this variation is consistent with a law of the form $D^n \propto t$ with n in the range -2 to $+3$.

Now, in the case of Cu_3Au alloy, it has been inferred by Poquette & Mikkola (1969) that the growth of antiphase domains is diffusion controlled with a rate process similar to that of grain growth in metals, *i.e.*

$$D^n - D_0^n = Kt \exp(-Q/k\theta),$$

where K is a constant, Q is the activation energy and θ is the temperature in K. If this form of dependence can be assumed with the present results for $t \geq 1$ minute, an activation energy for lithium ferrite of $3{\cdot}1 \pm 0{\cdot}8$ eV can be derived by comparing dD/dt for the two temperatures 700 and 730°C at the same value of D (*i.e.* when $t \sim 15$ min).

Some idea of the reliability of this estimate for the activation energy may be gained by appealing to the theoretical treatment of self-diffusion in the spinel group of compounds (Grimes, 1972), where the relation

$$Q \simeq 4\theta_D^2 md^2 \times 10^{-8} \text{ eV}$$

has been found to hold with θ_D the Debye temperature in K, m the mass of the diffusing species in atomic mass units and d the incremental jump distance in Å. At a domain boundary in lithium ferrite the important diffusion process is that involving the interchange of the Li^+ ion and one of the three Fe^{3+} ions in the tetrahedral group of octahedral cations. In this case the total activation energy will be given by the sum of the contributions from the Li^+ and Fe^{3+} ions, *i.e.*

$$Q \simeq 4\theta_D^2 (m_{Fe}\, d_{Fe}^2 + m_{Li}\, d_{Li}^2) \times 10^{-8} \text{ eV}.$$

Now when either of these ions migrates, it has the choice between passing through the edge or through the face of the surrounding octahedron of oxygen ions as illustrated in Fig. 9. In the former case migration would be directly to the next octahedral site, a jump distance of $a\sqrt{2}/4$, whilst in the latter, migration would take place *via* an adjacent tetrahedral site, *i.e.* two jumps of $a\sqrt{3}/8$ are needed.

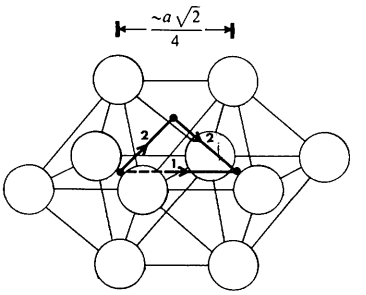

Fig. 9. Possible routes for migration between nearest-neighbour octahedral sites. Route 1, octahedral-to-octahedral site jump. Route 2, octahedral-to-tetrahedral-to-octahedral site jumps.

Thus, there are three simple ways by which a Li^+ and Fe^{3-} ion can interchange their positions and the corresponding activation energies are as follows:

Li^+ (Oct. → Tet. → Oct.) + Fe^{3+} (Oct. → Tet. → Oct.), $Q = 2{\cdot}14$ eV

Li^+ (Oct. → Oct.) + Fe^{3+} (Oct. → Tet. → Oct.), $Q = 2{\cdot}53$ eV

Li^+ (Oct. → Tet. → Oct.) + Fe^{3+} (Oct. → Oct.), $Q = 5{\cdot}32$ eV,

where the Debye temperature has been taken to be 512 K (Pollack & Atkins, 1962) and $a = 8{\cdot}33$ Å. The measured activation energy, therefore, is consistent with a diffusion mechanism in which the Fe^{3+} ion migrates *via* the somewhat easier route involving a neighbouring unoccupied tetrahedral site while the Li^+ ion moves directly between octahedral sites. It is worth mentioning, finally, that the measured activation energy for the self diffusion of Fe in Fe_3O_4 is 2·39 eV (Himmel, Mehl & Birchenall, 1953) which also lends credence to the present estimate, if allowance is made for some difference in Debye temperature, lattice parameter and the absence of Li^+ ions.

References

ANDERSON, P. W. (1956). *Phys. Rev.* **102**, 1008–1013.

BESSIERE, M., BLEY, M., CALVAYRAC, Y., LEFEBVRE, S. & FAYARD, M. (1976). *J. Appl. Cryst.* **9**, 353–354.

BOER, F. DE, VAN SANTEN, J. H. & VERWEY, E. J. W. (1950). *J. Chem. Phys.* **18**, 1032–1034.

BRAUN, P. B. (1952). *Nature (London)*, **170**, 1123.

BRUNEL, M. & DE BERGEVIN, F. (1964). *C.R. Acad. Sci.* **258**, 5628–5631.

BRUNEL, M. & DE BERGEVIN, F. (1966). *Solid State Commun.* **4**, 165–168.

CHEARY, R. W. & GRIMES, N. W. (1972*a*). *J. Appl. Cryst.* **5**, 57–63.

CHEARY, R. W. & GRIMES, N. W. (1972*b*). *Acta Cryst.* A**28**, 454–458.

GRIMES, N. W. (1972). *Philos. Mag.* **25**, 67–76.

HIMMEL, L., MEHL, R. F. & BIRCHENALL, C. E. (1953). *Trans. Metall. Soc. AIME*, **197**, 827–843.

KATO, E. (1958). *Bull. Chem. Soc. Jpn.* **31**, 113–117.
LANGFORD, J. I. (1968*a*). *J. Appl. Cryst.* **1**, 48–59.
LANGFORD, J. I. (1968*b*). *J. Appl. Cryst.* **1**, 131–138.
LEFEBVRE, S., PORTIER, R. & FAYARD, M. (1974). *Phys. Status Solidi A*, **24**, 79–89.
MARCINKOWSKI, M. J. & FISHER, R. M. (1960). *J. Appl. Phys.* **31**, 1687.
POINTON, A. J. & SAULL, R. C. (1969). *J. Am. Ceram. Soc.* **52**, 157–160.
POLLACK, S. R. & ATKINS, K. R. (1962). *Phys. Rev.* **125**, 1248–1254.
POQUETTE, G. E. & MIKKOLA, D. E. (1969). *Trans. Metall. Soc. AIME*, **245**, 743–751.
VISHNEVSKII, I. I., ALAPIN, B. G., LYSAK, S. V. & SKRIPAK, V. N. (1969). *Sov. Phys. Crystallogr.* **13**, 940–942.
WILSON, A. J. C. (1943). *Proc. R. Soc. London*, A**181**, 360–368.
WILSON, A. J. C. (1958). *Acta Cryst.* **11**, 227–228.
WILSON, A. J. C. (1962). *Proc. Phys. Soc. London*, **80**, 286–294.
WILSON, A. J. C. (1963). *Proc. Phys. Soc. London*, **81**, 41–46.
WILSON, A. J. C. (1965). *Proc. Phys. Soc. London*, **85**, 807–809.
WILSON, A. J. C. (1967). *Acta Cryst.* **23**, 888–898.
WILSON, A. J. C. (1970). *J. Appl. Cryst.* **3**, 71–73.
WILSON, A. J. C. & ZSOLDOS, L. (1966). *Proc. R. Soc. London*, A**290**, 508–514.
YAMAGUCHI, S., WATANABE, D. & OGAWA, S. (1961). *J. Phys. Soc. Jpn.* **17**, 1030–1041.

Acta Cryst. (1978). A**34**, 84–87

Influence of Polarization of the Incident Beam on Integrated Intensities in X-ray Energy-Dispersive Diffractometry

BY J. STAUN OLSEN, B. BURAS* AND T. JENSEN

Physics Laboratory II, *H. C. Ørsted Institute, University of Copenhagen, DK*-2100 *Copenhagen, Denmark*

AND O. ALSTRUP, L. GERWARD AND B. SELSMARK

Laboratory of Applied Physics III, *Building* 307, *Technical University of Denmark, DK*-2800 *Lyngby, Denmark*

(*Received* 4 *July* 1977; *accepted* 24 *July* 1977)

Polarization measurements of the primary X-ray beam produced by thick copper and tungsten anodes are reported and formulas derived for integrated intensities of Bragg reflections in energy-dispersive diffractometry with the polarization of the primary beam taken into account. It was found that for an angle of 45° between the scattering plane and the plane containing the electron beam and the primary beam, the influence of polarization vanishes, while it increases as the angle changes from 45° to either 0 or 90°. For the latter values, the influence of polarization is considerable at high photon energies and at scattering angles close to 90°.

1. Introduction

In conventional X-ray crystallographic studies, monochromatic characteristic radiation from the anode is used. It is unpolarized (in case of characteristic *K* X-radiation) and the polarization factors appearing in the formulas for integrated intensities – both for powders and single crystals – have the well known form arising from averaging the polarization factors for a linearly polarized beam over all possible directions of polarization (Zachariasen, 1945; Laue, 1960). In the energy-dispersive method, and sometimes also in double-crystal spectroscopy, the 'white' radiation (*Bremsstrahlung*) is used. It is well known that in the case of a thin target the white radiation is strongly polarized in the direction parallel to the electron beam incident on the target (Kuckuck & Ebert, 1973; Tseng & Pratt, 1973; and references therein). Our knowledge of polarization in the case of thick targets stems mainly from early measurements (Siegbahn, 1925; Ross, 1928; and references therein). Recently, Slivinsky (1971) measured the polarization of X-radiation emitted by commercial X-ray tubes with thick targets and found that it is strongly polarized in the direction parallel to the electron beam at the high-energy limit of the *Bremsstrahlung* spectrum, while the lower-energy X-rays exhibit a low but constant polarization in the same direction. However, to the best knowledge of the

* Also at Risø National Laboratory, DK-4000 Roskilde, Denmark.